ORIGINAL RESEARCH ARTICLE

DIVERSITY CONVERGES DURING COMMUNITY ASSEMBLY IN METHANOGENIC GRANULES, SUGGESTING A BIOFILM LIFE-CYCLE

Anna Christine Trego[1], Cristina Morabito[1], Simon Mills[1], Stephanie Connelly[2], Isabelle Bourven[3], Giles Guibaud[3], Christopher Quince[4], Umer Zeeshan Ijaz[2*], Gavin Collins[1,2*]

[1]School of Natural Sciences, National University of Ireland Galway, University Road, Galway, H91 TK33, Ireland.

[2]School of Engineering, University of Glasgow, Oakfield Avenue, Glasgow G128LT, United Kingdom.

[3]Groupement de Recherche Eau Sol Environnement, Faculté des Sciences Techniques, Université de Limoges, 123 Avenue Albert Thomas, 87060 Limoges Cedex, France.

[4]Warwick Medical School, University of Warwick, Gibbet Hill Road, Coventry CV4 7AL, United Kingdom.

***JOINT CORRESPONDING AUTHORS**

Umer Zeeshan Ijaz		**Gavin Collins**	
Tel:	+44(0)141-330-6458	Tel:	+353(0)91-493163
e-mail:	umer.ijaz@glasgow.ac.uk ,	e-mail:	gavin.collins@nuigalway.ie

Running Title: Life-cycle of anaerobic granules

Abstract

Anaerobic biological decomposition of organic matter is ubiquitous in Nature wherever anaerobic environments prevail, and is catalysed by hydrolytic, fermentative, acetogenic, methanogenic, and various other groups, including syntrophic bacteria. It is also harnessed in innovative ways in engineered systems that may rely on small (0.1-4.0 mm), spherical, anaerobic granules, which we have found to be highly-replicated, whole-ecosystems harbouring the entire community necessary to mineralise complex organics. We hypothesised distinct granule sizes correspond to stages in a biofilm life-cycle, in which small granules are 'young' and larger ones are 'old'. Here, granules were separated into 10 size fractions used for physico-chemical and ecological characterisation. Gradients of volatile solids, density, settleability, biofilm morphology, methanogenic activity, and EPS profiles were observed across size fractions. Sequencing of 16S rRNA genes indicated linear convergence of diversity during community assembly as granules increased in size. A total of 155 discriminant OTUs were identified, and correlated strongly with physico-chemical parameters. Community assembly across sizes was influenced by a niche effect, whereby *Euryarchaeota* dominated a core microbiome presumably as granules became more anaerobic. The findings indicate opportunities for precision management of environmental biotechnologies, and the potential of aggregates as playgrounds to study assembly and succession in whole microbiomes.

MAIN

Introduction

Global carbon cycling comprises not only primary production by photo- and chemo-synthesis on one hand, and carbon consumption by respiration on the other, but also relies fundamentally on the anaerobic, biological decomposition of organic matter wherever suitable environments prevail, such as in saturated wetlands; coastal, lake and marine sediments; and ruminant and termite guts, among many others [1–3]. Anaerobic digestion (AD) is a natural process mediated by the collective, sequential and cooperative action of several trophic groups of microorganisms, including hydrolytic bacteria, fermenters, organic-acid-oxidisers, and – finally – evolutionarily ancient, methanogenic archaea feeding on a narrow range of substrates including acetate, methanol and H_2/CO_2. Methanogenic consortia of this type comprise complex microbial communities of bacteria and archaea, and may include a diversity of syntrophic species, which operate within extremely narrow thermodynamic windows of profitability [4], as well as diversionary organisms – such as sulfate-reducing bacteria – competing with others for energy.

The AD process is widely harnessed for wastewater treatment in engineered, digester systems [5–7]. Many such digesters apply planktonic, suspended microbial cells to stabilise, and valorize, high-solids wastes, such as manures or crop-residues. Those are typically low-rate systems – applied under relatively low volumetric loading and, hence, across long hydraulic retention times so as to prevent washout from the digester of active cells. However, a distinct family of anaerobic digesters includes ‘retained-

biomass' systems based on the use of self-immobilised, biofilm granules, which settle quickly and, thus, avoid washout even from digesters applied under conditions of high volumetric loading and short hydraulic retention [8]. In this way, the use of anaerobic granules allows decoupling of hydraulic and biomass retention in anaerobic digesters, and such biofilms may be retained in AD systems for long periods of at least weeks or months.

Anaerobic granules, which were first discovered in the 1970s [9,10] and have since revolutionised the treatment of industrial wastewaters [11], are spherical biofilms of approximately 0.2-5 mm in diameter, each comprising a diverse microbial consortium, and each theoretically providing the entire microbial community necessary for complete mineralisation of complex organic feedstocks and wastes. The granular structure supports efficient transfer of substrates between trophic groups, as well as providing protection from toxins and environmental perturbations. Hulshoff Pol *et al.* [12] provided a pivotal review comparing mechanisms, and proposed a diversity of theories – based on ecology, physico-chemical features, and thermodynamics – to explain the granulation process, which all generally agreed that inert carriers likely play a critical role in granule formation, and that the early stages of granule development likely mimic the classical models of cell attachment and biofilm formation on solid surfaces [13,14]. Most authors also agree that *Methanosaeta concilii,* a methanogen with high acetate affinity, plays a key granulation role in providing a core of tangled filaments around which other cells aggregate. Whilst several studies focused on the earliest stages of

biofilm development, very few, however, studied growth and maturation of granules, and the microbiome, over time [12].

Indeed, many studies have described particle formation from diverse microbial communities, such as the bacterial colonization in the ocean of particulate organic matter [15], but the mechanisms by which complex communities assemble to form stable biofilms are still only poorly understood. Others describe the interaction of neutral and species-sorting processes, and the roles of generalists and specialists in community assembly [16].

Whilst full-scale anaerobic digesters (with volumes of typically up to several hundred cubic metres) contain millions of single-granule ecosystems, not all granules are the same. Ahn [17] found the typical range of granule diameters to be 0.1-5 mm, and in a characterisation by Diaz *et al.* [18] different granule morphologies were observed from single digesters. They separated granules by colour, and differences were observed in granule size and structure. Nonetheless, our recent research has indicated that granules from within distinct size ranges harbour statistically identical microbiomes [19], even though the community structure in granules of different sizes may differ. Each individual granule therefore represents a perfectly parameterised, whole biofilm ecosystem. Thus – and rather uniquely in either Nature or the built environment – anaerobic granules may well be considered as distinct, replicated, whole microbial communities.

114 This may pose an opportunity to test questions about community assembly; growth
115 patterns; and drivers of community structure and diversity in complex biofilms –
116 including as encouraged by Rillig *et al.* [20], who proposed soil aggregates as massively
117 concurrent evolutionary incubators. The utility of such highly-replicated, whole-
118 microbial-communities to study microbial evolution should be explored. For example,
119 the extent to which ecological theories hold across the expansion of, and succession in,
120 the microbial community in granules should provide useful information for the
121 management of environmental biotechnologies. Moreover, whether the granulation
122 process is cyclical, and follows a predictable life cycle, is an important question for both
123 environmental engineering and microbial ecology.
124
125 We hypothesise that differently sized granules represent different stages of biofilm
126 development and that granules taken from a single digester at a single point in time,
127 having survived the same environmental conditions, may, in fact, represent different
128 stages of growth over a biofilm life-cycle where the smallest granules are at the earliest
129 stages of formation and the largest granules are the oldest and most mature. We
130 attempted an intensive characterisation of anaerobic granules from a full-scale digester
131 across multiple, discrete size fractions, to characterise morphological, physico-chemical,
132 physiological and ecological differences across a set of highly-resolved granule size
133 fractions. This provides an interesting new perspective for Microbial Ecology with
134 respect to community assembly, biofilm development, and the drivers of microbial
135 diversity in a controlled system underpinned by collections of single, whole-ecosystem
136 aggregates.

Materials and Methods

Source of biomass and size fractionation

Anaerobic sludge granules were obtained from a full-scale, mesophilic (37°C) upflow anaerobic sludge bed (UASB) digester treating potato-processing wastewater in the Netherlands. The sludge was size-separated into ten discrete size fractions (A-J) by passing the granules through a series of stainless-steel sieves. Each fraction was suspended in 1X phosphate buffered saline (PBS; Fisher Scientific, Geel, Belgium), sparged with N_2 gas, and allowed to settle for 1 h before determining the settled volume.

Total, and volatile, solids; and sludge settling velocity, and density

The total solids (TS) and volatile solids (VS) concentrations of granules from each size fraction were determined using the standard loss-on-ignition technique [21]. The settling velocity, and density, of granules (n=10) from each size fraction, A-J, was determined. A 1-m long, clear, acrylic tube, fitted with a stopper at one end was fastened vertically and filled with deionised water. Two markings were made on the outside of the tube, at 0.3 m and 0.6 m from the top, and the water temperature was recorded. The diameter of individual granules was measured using electronic digital calipers. Granules were individually dropped into the column of water, and the time (seconds) required for each granule to travel 0.3 m (the distance between the two markings) was measured. The settling velocity was the distance (0.3 m) divided by settling time. Stokes' Law was then applied to determine granule density.

Scanning electron microscopy (SEM)

Three granules from each size fraction were randomly selected for SEM imaging. Granules were placed in clean, individual 1.5-ml microcentrifuge tubes and covered with 2.5% (w/v) glutaraldehyde in 0.5 M cacodylate buffer (pH 7.2). The tubes were inverted gently and incubated overnight at 4°C. The supernatant was removed and granules were washed three times in 1X PBS, before being dehydrated by passing through a series of 10-min ethanol washes using 50%, 70% and 90% ethanol. Dehydrated granules were placed on carbon tabs, which were then fastened to aluminum stubs. An aliquot of 25 µl hexamethyldisilazane (HMDS) was placed on each granule, under a fume hood, and allowed to dry overnight. Specimens were gold-sputtered and imaged in a scanning electron microscope (Hitachi S-2600, Mountain View, CA, USA).

Extraction and characterisation of extracellular polymeric substances (EPS)

Loosely bound (LB) and tightly bound (TB) EPS was extracted in duplicate from sludge from each size fraction using the cation exchange resin (CER) technique [22,23]. Colorimetric assays were used to investigate the biochemical composition of the EPS using a spectral photometer (Cadas 50 S, Dr Lange, Berlin, Germany). Concentrations of proteins and humic-like substances (HLS) were determined and corrected [24,25]. Bovine serium albumin (96%, Sigma-Aldrich, St. Louis, Missouri, USA) was used as a standard for proteins and humic acids (Sigma-Aldrich, St. Louis, Missouri, USA) as the standard for HLS. Polysaccharides were measured following DuBois *et al.* [26], using a glucose standard.

183

184 *Specific methanogenic activity (SMA)*

185 An SMA buffer solution was prepared in a round-bottom flask by combining 0.4 ml
186 0.0001% (w/v) resazurin (Fisher Scientific, Geel, Belgium), 0.56 g cysteine
187 hydrochloride monohydrate and enough distilled water (dH2O) to bring the volume to
188 700 ml. The pH was adjusted to 7.0-7.1 by dropwise addition of 8 M NaOH, and the final
189 volume was adjusted to 1 L. The solution was boiled until clear, and immediately sealed
190 and cooled on ice with constant N_2 sparging until at 50ºC when 3.05 g sodium
191 bicarbonate were added before sealing the flask. The SMA buffer was added with
192 sludge granules to 60-ml, glass bottles to give a final volume of buffer and granules of
193 10 ml, and a final VS concentration of 4 g L^{-1}. The bottles were sealed and N_2 -flushed
194 before acclimatisation at 37ºC for 48 h. Aliquots of 0.1 ml soluble substrates were then
195 added to separate, respective bottles to give final concentrations of 30 mM acetate, 15
196 mM butyrate or 30 mM propionate. No-substrate controls measured background activity.
197 To test for autotrophic methanogenesis, H_2/CO_2 (80:20, v/v) was added at 1 bar for 20
198 s. N_2/CO_2 (80:20, v/v) was used to control H_2-fed assays. Headspace biogas pressure
199 was measured as millivolts (mv), using a handheld pressure transducer (CentrePoint
200 Electronics, Galway, Ireland), and converted to biogas volume (ml) using a headspace
201 correction factor [27,28]. Gas chromatography (CP-3800, VARIAN Inc., Walnut Creek,
202 CA) was used to determine the methane concentration (%) in the biogas, and the
203 accumulation rate was plotted. The precise, *in situ* concentration of VS in each bottle
204 was determined by drying and burning, as before. In the case of soluble substrates,
205 SMAs were determined under STP conditions as the daily rate of methane production

as a function of the total VS. SMA for gaseous substrates were calculated using a similar approach; however, the rate was computed using the reaction stoichiometry of 4:1 molar of H_2 consumption to methane production.

DNA Extraction

A mass of 0.1 g wet sludge from each of the size fractions was weighed into respective, sterile tubes in triplicate. DNA was extracted on ice following the DNA/RNA co-extraction method described by Griffiths *et al*. [29], which is based on bead beating in 5% (w/v) cetyl trimethylammonium bromide (CTAB) extraction buffer, followed by phenol-chloroform extraction. Integrity of nucleic acids was assessed using a nanodrop (Thermo Fisher Scientific, Waltham, MA, USA). Concentrations were determined using a Qubit fluorometer (Invitrogen, Carlsbad, CA, USA) and normalised to 5 ng DNA μl^{-1} before storage at -80ºC.

High-throughput DNA Sequencing, Bioinformatics, and Statistical Analysis

Amplification of the 16S rRNA gene sequences was performed by The Foundation for the Promotion of Health and Biomedical Research of Valencia Region, FISABIO (Valencia, Spain) using the universal bacterial and archaeal primer set: forward primer 515F and reverse primer 806R. The resulting amplicon library of short inserts was sequenced on the Illumina MiSeq platform. Abundance tables were generated by constructing OTUs (as a proxy for species). Statistical analyses were performed in R using the combined data generated from the bioinformatics as well as meta data associated with the study. Details are described further in Supplementary Methods.

Results

Distribution of granule sizes

A normal distribution of granule sizes was observed with a majority (>75%) of the sludge volume comprising medium-range granules (fractions D – G; Fig. 1). No granules >4 mm were found. The VS proportion of TS was relatively high (average, 91.8%; σ^2, 0.88) in granules from medium and larger fractions (D – J) but lower in smaller granules (86.2%, 70.4% and 89.0% in fractions A, B and C, respectively).

Granule ultrastructure

A clear gradient in aggregate ultrastructure was apparent across the size fractions (Fig S1). The smallest biofilms (Fractions A – C) presented as 'flakes'; medium-sized granules (Fractions D – F) appeared better defined but were 'flat' (i.e. not spherical); larger granules (Fractions G – I) were distinctly spherical and more 'granular'; and in the largest granules (Fraction J), large cracks and void spaces were apparent, and the granules appeared to have broken apart, losing structural integrity (Fig. 1).

Density and settleability

The density and settling velocity of granules were broadly linear across the size fractions (Fig. 1), but were inversely related: smaller granules (Fraction A) had high densities (104.6 g/cm^3) but low settling velocities (average, 0.001 m/s), whilst large granules (Fraction J) were less dense (6.82 g/cm^3) and more settleable (average, 0.041 m/s).

252

253 *SMA across sizes*

254 Granules from across all sizes were more methanogenically active against hydrogen
255 than against the volatile fatty acid substrates tested (Fig. 1). Larger granules (Fractions
256 H and I) were less active than smaller granules, regardless of substrate. Medium-sized
257 granules (Fractions E – G) were generally the most active against all substrates.

258

259 *EPS composition across granule sizes*

260 There was no change in composition of tightly-bound (TB)-EPS across the size fractions
261 – the proportion of each of the three examined components (protein, 53.2% (σ^2, 7.1);
262 humic-like substances (HLS), 23.0% (σ^2, 7.5); and polysaccharides, the remaining
263 23.7% (σ^2, 2.8)) was relatively stable. However, a gradient was apparent across the size
264 fractions in the proportions of loosely-bound (LB)-EPS components; for example, the
265 proportions of proteins and polysaccharides were high, and HLS were low, in small
266 granules, whilst the obverse was the case for large granules (Fig. 1).

267

268 *Microbial composition and diversity across size fractions*

269 Amplicon sequencing data analysis for the ten separate size fractions (n = 30 samples)
270 resulted in, from each fraction: 2 927 OTUs from an average of 71 772 ± 18 691 initial
271 paired-end reads, 71 345 ± 18 596 reads prior to quality trimming with Sickle, and 53
272 239 ± 14 453 paired-end reads capable of being overlapped using PandaSeq.

273

Alpha diversity analysis indicated a strong, linear diversity gradient across the size fractions with significantly ($p = 0.00019$) higher rarefied richness in the smaller granules (Fraction A) than in the larger granules (Fraction J), and with significant differences between nearly every combination of fractions. Similarly, for Shannon entropy, small granules housed much more diverse communities than larger granules ($p = 0.00012$ between Fractions A and J), and there were significant differences between nearly every possible combination of fractions. Beta diversity analysis revealed a highly significant ($p = 0.001$) differentiation pattern across Fractions A to J using the Bray-Curtis ($p = 0.001$), unweighted UniFrac (Fig. S2), and the weighted UniFrac distance metrics (Fig. 2; $p = 0.001$).

Archaea from the most abundant taxa (Fig. 2) were dominated by the two acetoclastic methanogens from the genus *Methanosaeta*; hydrogenotrophic methanogens from the genera *Methanolinea* and *Methanobacterium*; and the metabolically-diverse methanogens from the family *Methanosarcinaceae*. The 10 most abundant organisms included an interesting and diverse bacterial population: *Hyd24-12*, a candidate phylum in the Fibrobacteres-Chlorobi-Bacteroidetes superphylum; bacteria from the uncultured *Phycisphaerae* lineage; and the highly diverse *Nitrospirales* order. A gradual gradient in the relative abundance of the top-25 most abundant OTUs was observed across the size fractions (A to J), where the top-25 constituted 49.45% of the community in Fraction A but 78.48% of the community in Fraction J. Interestingly, the four most abundant OTUs, which were relatively more abundant with granule size, were all methanogenic archaea: *Methanosaeta* (5.71 ± 0.40% to 16.56 ± 0.42%), *Methanolinea*

297 (4.30 ± 0.07% to 8.36 ± 2.01%), and two distinct classifications of *Methanobacterium*
298 *beijingense* (2.31 ± 0.42% to 9.34 ± 1.28%; and 2.2 ± 0.42% to 9.41 ± 1.15%). The
299 relative abundance of those methanogens, as a group, increased from 14.53% in
300 Fraction A to 43.67% in Fraction J – nearly half of the entire microbial community.
301
302 NRI and NTI analyses provided U-shaped gradients across the size fractions (Fig 2).
303 The smallest and largest granules clustered together phylogenetically (positive values)
304 and were therefore more influenced by environmental factors. Meanwhile, the medium-
305 sized granules (Fractions E – G) has slightly negative NRI values – tending towards
306 phylogenetic dispersion.
307
308 *Discriminant OTUs across sizes*
309 Despite originating from the same environmental conditions, the overall community
310 structure was observed to be significantly different between Fractions A – J and sPLS
311 analysis identified 155 discriminant OTUs responsible for the observed changes (Fig.
312 3). Fourteen of the discriminant OTUs were methanogens, whilst all others were
313 bacteria. There were three distinct groupings according to abundance, and across
314 sizes: 41.3% of the discriminant OTUs were 'upregulated' in the smallest granules, 9%
315 in the medium size fractions, and 49.7% in the largest size fractions.
316
317 *Correlations between physico-chemical differences and community structure*
318 Strong positive and negative correlations were observed, based on granule size,
319 between the 155 discriminant OTUs and the physico-chemical data (Fig. 4). The OTUs

320 which were upregulated in the small granule fractions (A – C) showed strong positive
321 correlations with density, and LB-EPS protein and polysaccharides. Discriminant OTUs
322 in the medium-sized granules correlated significantly with SMA against acetate,
323 propionate, butyrate and hydrogen – although, intriguingly, none of those OTUs were
324 methanogenic archaea, indicating that various syntrophic and fatty-acid-oxidising
325 bacteria may have been discriminant taxa in medium granules. There was a clear
326 distinction in how OTUs upregulated in the medium-sized (Fractions D – G) and smaller
327 granules correlated with meta-data. Correlations between upregulated OTUs in
328 medium-sized granules and density, and settling velocity, were less significant than in
329 small granules. The medium-sized granules appeared to represent the site of a
330 transition zone, between small and larger granules, where the nature of such
331 correlations shifted (from positive to negative, or *vice versa*). OTUs upregulated in the
332 large granules (Fractions H – J) strongly positively correlated with settling velocity, and
333 negatively correlated with SMA against hydrogen and butyrate.
334
335 *Euryarchaeota dominate*
336 Although the community proportion of *Euryarcheota* increased with granule size, the
337 entire group comprised only 69 OTUs in total, and was therefore not very diverse (Fig
338 5), which had the effect of reducing the total richness of the community in bigger
339 granules (i.e. presumably, as granule size increases). This was tested by calculating the
340 rarefied richness of the *Euryarcheota*, which was found to be fixed with granule size. In
341 other words, although the rarefied richness fluctuated slightly, there was no trend

342 toward reduced diversity within this phylum, which appeared to dominate as granules
343 matured.
344
345 **Discussion**
346 One of the primary objectives of this study was to intensively characterise anaerobic
347 granules from across a series of discrete sizes to identify drivers of community
348 assembly during biofilm maturation. We hypothesised that distinct granule sizes
349 correspond to stages in a biofilm life-cycle, in which small granules are 'young' and
350 larger ones are 'old'. Across each parameter explored, there were significant differences
351 between granules of different sizes. As far we are aware, no such study has been
352 reported before.
353
354 Volatile solids comprised a smaller proportion of the biofilms in fractions A – C. One of
355 the key theories on granulation is the '*spaghetti theory*', which proposes that during the
356 initial stages of biofilm formation cells attach to inorganic nuclei [30,31], which may have
357 made up an inorganic core comprising a larger proportion of the solids in the smaller
358 granules. As further cells attach, and the biofilm grows, the organic fraction would
359 become more important in larger granules, which is supported by the VS data
360 presented.
361
362 A distinct gradient was observed in the ultra-structural features across the size fractions.
363 Small granules were flaky and undefined, whilst the largest granules were spherical and
364 – in some cases – beginning to break apart. Gradients in density and settleability

365 profiles were also observed across size, whereby smaller granules were much more
366 dense than larger granules, but had much lower settling velocities. Diaz *et al*. [18] also
367 applied SEM using granules they had sliced in half revealing cross-sections, observing
368 that largest granules had major cracks, and void spaces, that were less apparent in
369 smaller granules. It is possible that such differences, or changes, in the structure of the
370 granules also affects density: as granules become larger they acquire more cracks,
371 channels and void spaces due to gas diffusion from the biofilm interior, which in turn
372 renders the biofilm less tightly packed and – consequently – less dense. Furthermore,
373 previous studies have described stratification of the sludge bed in anaerobic digesters
374 using granules, where larger granules occupy the bottom and smaller ones the top of
375 the bed [32–34] – this is interesting if granules in a bioreactor are to be considered as a
376 meta-community or meta-organism. More specifically, however, avoiding biomass
377 wash-out is a key consideration in applying anaerobic granules in bioreactors, and the
378 findings lead us to conclude that settleability, rather than density, is the driving force for
379 stratification.
380
381 There appears to have been a clear, linear gradient characterised by reducing diversity
382 and converging community structure across the size fractions, from small to large,
383 which was presumably across community assembly and biofilm maturation. This was
384 somewhat counter to our initial assumption, which was that as the biofilm assembles
385 and matures, diversity and rarefied richness would increase, especially as the biofilm
386 simply contained significantly more cells. Both rarefied richness and diversity (measured
387 by Shannon entropy) decreased significantly with granule size, due to the gradual

388 dominance of a sub-group of the OTUs. Interestingly, the dominant, core group
389 appeared to be comprised of four methanogenic archaea: *Methanosaeta*, *Methanolinea*,
390 and two classifications of *Methanobacterium beijingense,* which are mainly
391 hydrogenotrophic methanogens and may explain the high methanogenic activity
392 measured against hydrogen.
393
394 *Methanosarcinaceae* were also present, which are able to metabolise a wide range of
395 substrates including methylated amines, methanol, H_2/CO_2, acetate, dimethyl sulfide,
396 methanethiol and sometimes carbon monoxide [35]. Abundant bacteria included the
397 candidate phylum *Hyd24-12*, which are globally distributed but commonly found in
398 anaerobic digesters where they are likely key fermenters, producing acetate and H_2
399 from sugars [36], and supporting the metabolisms of the methanogens and
400 *Nitrospirales*, which are the predominant nitrite-oxidisers playing critical roles in the
401 biogeochemical cycling of nitrogen [37].
402
403 Sacchrolytic fermenters comprised a vast majority of the discriminant OTUs, with only a
404 few notable exceptions. Within the subgroup of discriminant OTUs upregulated in the
405 small granules, three were known, or likely, parasites: bacteria from the TM6 lineage;
406 the *Parcubacteria* and a genus of Proteobacteria; and *Bdellovibrio* [38,39]. In the group
407 of discriminants upregulated in the medium-sized granules, notable taxa included
408 *Desulfobulbus*. Of the *Desulfobulbus* species to have thus far been isolated, all come
409 from anaerobic environments with one particular species, the syntroph *Desulfobulbus*
410 *propionicus*, capable of propionate oxidation with a methanogenic partner [40,41]. Other

411 members of the genus are only known to be primary fermenters. The subgroup of
412 discriminant OTUs upregulated in the large granules contained many of the top-25
413 most-abundant OTUs – constituting the emergence of a core microbiome. This group
414 additionally included several syntrophic bacteria, such as *Syntrophorhabdus*,
415 *Methanomethylovorans*, *Syntrophobacter* and *Desulfomicrobium* among others. Those
416 syntrophs generally are sulfate-reducers found in habitats ranging from marine
417 sediments to anaerobic digesters [42,43]. Finally, the largest granules contained the
418 majority of the discriminant OTUs classified as *Euryarchaeota.* One OTU, in particular,
419 was identified as *Methanolinea*, hydrogenotrophic methanogens in the top-25 most-
420 abundant OTUs, and which were significantly positively correlated with SMAs against
421 acetate and propionate.
422
423 Three alternative explanations may address the nature of the community assembly, and
424 decreasing diversity, evident in the granules from across the size fractions studied. The
425 first is based on the *neutral explanation* i.e. that communities are a balance between
426 immigration and extinction [44]. In that case, reduced microbial immigration would result
427 in reduced diversity. The second is based on the number of *functional groups* present in
428 samples from across the size fractions studied. The relative abundance of distinct
429 methanogenic archaea appeared to have increased with granule size, but since that
430 functional group was not very diverse richness would be curtailed. The final hypothesis
431 is based on a *competition effect* whereby better competitors would dominate functional
432 groups and lead to reduced diversity in granules from across the sizes.
433

Our analysis determined *Euryarchaeota* as the increasingly-dominating group along the gradient of granule sizes, from small to large, but that diversity in the group was low. This indicates that the decreasing richness observed was a phenomenon associated with changing proportions of functional groups rather than with reduced diversity inside groups. The basic neutral model ignores any functional differences between organisms and treats the community purely as a balance between immigration and extinction. What is more likely is that there are functional niches whose abundance can change over time according to conditions. Within those groups, neutrality may, indeed, operate adding additional ecological complexity. However, and due to the complexity of the biofilm formation and maturation, the neutral model alone cannot simply explain assembly or diversity. Indeed, granules may become more strictly anaerobic with increasing size, creating ideal conditions for methanogenic populations to expand.

The observations from this study – on gradients in ultrastructure, activity, EPS composition and community structure – culminate in the proposal of a life-cycle model for anaerobic granular biofilms. This model (Fig. 2) proposes that granules begin as very small, compact and structurally-irregular, yet diverse, agglomerations of cells. Such granules are considered to be ‘young’. As the biofilm ages, it grows into a medium-sized, highly-active, structurally-stable entity with a less-diverse community structure, selecting rather for a community capable of efficient methane generation i.e. a consortium completing the anaerobic digestion process without significant accumulation of intermediate by-products. We consider those granules to be ‘ripe’. Further aging weakens the granule structure, and cracks and voids form. Activity decreases, likely due

457 to structural inefficiencies in mass transport of substrates from one trophic group to
458 another, but the diversity continues to converge primarily toward a methanogenic
459 consortium. The granules may then be considered as 'mature'. It is probable then, that
460 the granules eventually break apart, but that the small fragments are still comprised of
461 an active consortium and form the basis for new 'young' granules. The only observation
462 that does not fully support this hypothesis is the set of observed gradients in rarefied
463 richness and diversity – the linearity of the gradients does not necessarily indicate a
464 circular trajectory – leading to the question, *what exactly is the fate of a large granule?*
465 And, what is happening between, in this study, fractions J and A? In particular, the
466 source of the additional richness in Fraction A is unclear, but it is likely that the
467 surrounding medium (of wastewater, in the case of bioreactors) will provide the
468 necessary additional diversity to cultivate new young granules.
469
470 Interestingly, medium-sized granules contributed a volumetric majority to the biomass
471 used for this experiment. Those were also the most methanogenically active granules
472 and appeared to have the most 'stable' ultrastructure. This indicates that the medium-
473 sized granules may be the most stable; least open to immigration; and most important
474 for methane production. Additionally, our NRI and NTI analyses demonstrated that the
475 community structure of medium-sized granules was least influenced by environmental
476 stresses. Equally, however, the smallest and largest fractions clustered together with
477 NRI and NTI analysis, indicating that both were more vulnerable to change and
478 environmental influence – and supporting somewhat the idea that both occupy pivotal
479 points of change on a potential biofilm life 'cycle'.

Moreover, the alpha diversity analysis showed that medium-sized granules were perhaps optimally diverse – containing a community rich in methane-producing archaea, but not over-dominated by them. It is possible then, that the digester system may self-regulate to select for medium-sized granules as a type of optimal growth phase in which critical trophic groups are maintained, suggesting the use of sophisticated ecological survival strategies. Furthermore, this may point to potential management strategies for digester operation where systems are managed to promote the emergence and existence of medium-sized granules.

Conclusions

In summary, ecophysiolological and physico-chemical gradients were apparent in methanogenic granules across the highly-resolved set of size fractions investigated, indicating that aggregate size matters for both structure and function. It appeared that, as such biofilms developed, the microbial community significantly lost diversity. We conclude that this was associated with low-diversity, functional groups – in in this case the *Euryarchaeota* – becoming more dominant, due to a niche functional effect as developing granules became more anaerobic. The methanogens comprised the majority of a core microbiome across the life-stages of anaerobic granules. Medium-sized granules may be optimal in terms of structure and function, and granules may follow a biofilm life-cycle that self-selects for mostly medium-sized granules in a meta-organism that also includes smaller and larger aggregates. Indeed, the idea that operating a digester toward further selecting for medium-sized granules might result in optimally

503 efficient conversions and bioenergy production. Finally, such granules provide ideal
504 playgrounds to study community assembly, expansion, and succession of complex
505 biofilm microbiomes, as well as very-high-throughput studies to investigate the response
506 of replicated, whole microbial communities to environmental parameters and change.
507
508
509
510
511
512 **References**

513 1. Freeman C, Ostle N, Kang H. An enzymic 'latch' on a global carbon
514 store. Nature [Internet]. 2001 Jan 11;409:149. Available from:
515 http://dx.doi.org/10.1038/35051650
516 2. Chapelle FH, O'Neill K, Bradley PM, Methé BA, Ciufo SA, Knobel LL, et al. A
517 hydrogen-based subsurface microbial community dominated by methanogens.
518 Nature [Internet]. 2002 Jan 17;415:312. Available from:
519 http://dx.doi.org/10.1038/415312a
520 3. Martin W, Müller M. The hydrogen hypothesis for the first eukaryote. Nature
521 [Internet]. 1998 Mar 5;392:37. Available from: http://dx.doi.org/10.1038/32096
522 4. Dolfing J, Larter SR, Head IM. Thermodynamic constraints on methanogenic
523 crude oil biodegradation. Isme J [Internet]. 2007 Dec 13;2:442. Available from:
524 http://dx.doi.org/10.1038/ismej.2007.111
525 5. Appels L, Lauwers J, Degrève J, Helsen L, Lievens B, Willems K, et al. Anaerobic

digestion in global bio-energy production: Potential and research challenges. Renew Sustain Energy Rev [Internet]. 2011;15(9):4295–301. Available from: http://www.sciencedirect.com/science/article/pii/S1364032111003686

6. Seghezzo L, Zeeman G, van Lier JB, Hamelers HVM, Lettinga G. A review: The anaerobic treatment of sewage in UASB and EGSB reactors. Bioresour Technol [Internet]. 1998;65(3):175–90. Available from: http://www.sciencedirect.com/science/article/pii/S0960852498000467

7. van Lier JB, van der Zee FP, Frijters CTMJ, Ersahin ME. Celebrating 40 years anaerobic sludge bed reactors for industrial wastewater treatment. Rev Environ Sci Bio/Technology [Internet]. 2015;14(4):681–702. Available from: https://doi.org/10.1007/s11157-015-9375-5

8. Kato MT, Rebac S, Lettinga G. Anaerob c Treatment of of Low-Strength Brewery Wastewater in Expanded Granular Sludge Bed Reactor. Appl Biochem Biotechnol. 1998;76.

9. Lettinga G, van Velsen AFM, Hobma SW, de Zeeuw W, Klapwijk A. Use of the upflow sludge blanket (USB) reactor concept for biological wastewater treatment, especially for anaerobic treatment. Biotechnol Bioeng [Internet]. 1980 Sep 11;22(4):699–734. Available from: https://doi.org/10.1002/bit.260220402

10. Ir R, Lettinga G. Anaërobe zuivering van het afvalwater van de bietsuikerindustrie (2)*. 1976;0(2):1–6.

11. van Lier JB, Tilche A, Ahring BK, Macarie H, Moletta R, Dohanyos M, et al. New perspectives in anaerobic digestion. Water Sci Technol [Internet]. 2001 Jan 1;43(1):1–18. Available from: http://dx.doi.org/10.2166/wst.2001.0001

12. Hulshoff Pol LW, de Castro Lopes SI, Lettinga G, Lens PNL. Anaerobic sludge granulation. Water Res [Internet]. 2004;38(6):1376–89. Available from: http://www.sciencedirect.com/science/article/pii/S0043135403006705
13. Stoodley P, Sauer K, Davies DG, Costerton JW. Biofilms as Complex Differentiated Communities. Annu Rev Microbiol [Internet]. 2002 Oct 1;56(1):187–209. Available from: https://doi.org/10.1146/annurev.micro.56.012302.160705
14. Hall-Stoodley L, Costerton JW, Stoodley P. Bacterial biofilms: from the Natural environment to infectious diseases. Nat Rev Microbiol [Internet]. 2004 Feb 1;2:95. Available from: http://dx.doi.org/10.1038/nrmicro821
15. Datta MS, Sliwerska E, Gore J, Polz MF, Cordero OX. Microbial interactions lead to rapid micro-scale successions on model marine particles. Nat Commun [Internet]. 2016;7(May):1–7. Available from: http://dx.doi.org/10.1038/ncomms11965
16. Langenheder S, Székely AJ. Species sorting and neutral processes are both important during the initial assembly of bacterial communities. Isme J [Internet]. 2011 Jan 27;5:1086. Available from: http://dx.doi.org/10.1038/ismej.2010.207
17. Ahn Y. Physicochemical and microbial aspects of anaerobic granular biopellets. J Environ Sci Heal Part A [Internet]. 2000 Oct 1;35(9):1617–35. Available from: https://doi.org/10.1080/10934520009377059
18. Díaz EE, Stams AJM, Amils R, Sanz JL. Phenotypic properties and microbial diversity of methanogenic granules from a full-scale upflow anaerobic sludge bed reactor treating brewery wastewater. Appl Environ Microbiol. 2006;72(7):4942–9.
19. Trego AC, O'Sullivan S, Mills S, Porca E, Ijaz UZ, Collins G. Highly-replicated,

whole-microbial communities in single anaerobic sludge granules respond reproducibly and distinctly to environmental cues. bioRxiv. 2018;

20. Rillig MC, Muller LAH, Lehmann A. Soil aggregates as massively concurrent evolutionary incubators. Isme J [Internet]. 2017 Apr 14;11:1943. Available from: http://dx.doi.org/10.1038/ismej.2017.56

21. APHA. Standard methods for the examination of water and wastewater. 21st ed. New York: American Public Health Association, Washington DC; 2005.

22. Frølund B, Palmgren R, Keiding K, Nielsen PH. Extraction of extracellular polymers from activated sludge using a cation exchange resin. Water Res. 1996;30(8):1749–58.

23. D'Abzac P, Bordas F, Van Hullebusch E, Lens PNL, Guibaud G. Extraction of extracellular polymeric substances (EPS) from anaerobic granular sludges: Comparison of chemical and physical extraction protocols. Appl Microbiol Biotechnol. 2010;85(5):1589–99.

24. Lowry, Oliver; Rosebrough, Nira; Farr ,A. Lewis & Randall R. Protein Measurement With The Folin Phenol Reagent. J Biol Chem [Internet]. 1951;193(1):265–75. Available from: http://www.life.illinois.edu/biochem/355/articles/LowryJBC193_265.pdf

25. Frølund B, Griebe T, Nielsen PH. Enzymatic activity in the activated-sludge floc matrix. Appl Microbiol Biotechnol. 1995;43:755–61.

26. DuBois M, Gilles KA, Hamilton JK, Rebers PA, Smith F. Colorimetric Method for Determination of Sugars and Related Substances. Anal Chem [Internet]. 1956 Mar 1;28(3):350–6. Available from: https://doi.org/10.1021/ac60111a017

595 27. Colleran E, Concannon F, Golden T, Geoghegan F, Crumlish B, Killilea E, et al.
596 Use of Methanogenic Activity Tests to Characterize Anaerobic Sludges, Screen
597 for Anaerobic Biodegradability and Determine Toxicity Thresholds against
598 Individual Anaerobic Trophic Groups and Species. Water Sci Technol [Internet].
599 1992 Apr 1;25(7):31 LP-40. Available from:
600 http://wst.iwaponline.com/content/25/7/31.abstract
601 28. Coates JD, Coughlan MF, Colleran E. Simple method for the measurement of the
602 hydrogenotrophic methanogenic activity of anaerobic sludges. J Microbiol
603 Methods [Internet]. 1996;26(3):237–46. Available from:
604 http://www.sciencedirect.com/science/article/pii/0167701296009153
605 29. Griffiths RI, Whiteley AS, O'Donnell AG, Bailey MJ. Rapid Method for
606 Coextraction of DNA and RNA from Natural Environments for Analysis of
607 Ribosomal DNA- and rRNA-Based Microbial Community Composition. Appl
608 Environ Microbiol [Internet]. 2000 Dec 5;66(12):5488–91. Available from:
609 http://www.ncbi.nlm.nih.gov/pmc/articles/PMC92488/
610 30. Weignant W. The "spagetti theory" on anaerobic sludge formation, or the
611 inevitability of granulation. In: Lettinga G, Sehnder A, Grotenhuis J, Hulshoff Pol
612 L, editors. Granular anaerobic sludge: microbiology and technology. THe
613 Netherlands: Pudoc. Wageningen; 1987. p. 146–52.
614 31. Jian C, Shi-yi L. Study on Mechanism of Anaerobic Sludge Granulation in UASB
615 Reactors. Water Sci Technol [Internet]. 1993;28(7):171–8. Available from:
616 http://wst.iwaponline.com/content/28/7/171
617 32. Yan Y-G, Tay J-H. Characterisation of the granulation process during UASB start-

up. Water Res [Internet]. 1997;31(7):1573–80. Available from: http://www.sciencedirect.com/science/article/pii/S0043135496003545

33. Torkian A, Eqbali A, Hashemian SJ. The effect of organic loading rate on the performance of UASB reactor treating slaughterhouse effluent. Resour Conserv Recycl [Internet]. 2003;40(1):1–11. Available from: http://www.sciencedirect.com/science/article/pii/S0921344903000211

34. Connelly S, Shin SG, Dillon RJ, Ijaz UZ, Quince C, Sloan WT, et al. Bioreactor Scalability: Laboratory-Scale Bioreactor Design Influences Performance, Ecology, and Community Physiology in Expanded Granular Sludge Bed Bioreactors. Front Microbiol [Internet]. 2017;8:664. Available from: https://www.frontiersin.org/article/10.3389/fmicb.2017.00664

35. Oren A. The Family Methanosarcinaceae BT - The Prokaryotes: Other Major Lineages of Bacteria and The Archaea. In: Rosenberg E, DeLong EF, Lory S, Stackebrandt E, Thompson F, editors. Berlin, Heidelberg: Springer Berlin Heidelberg; 2014. p. 259–81. Available from: https://doi.org/10.1007/978-3-642-38954-2_408

36. Kirkegaard RH, Dueholm MS, McIlroy SJ, Nierychlo M, Karst SM, Albertsen M, et al. Genomic insights into members of the candidate phylum Hyd24-12 common in mesophilic anaerobic digesters. Isme J [Internet]. 2016 Apr 8;10:2352. Available from: http://dx.doi.org/10.1038/ismej.2016.43

37. Daims H. The Family Nitrospiraceae BT - The Prokaryotes: Other Major Lineages of Bacteria and The Archaea. In: Rosenberg E, DeLong EF, Lory S, Stackebrandt E, Thompson F, editors. Berlin, Heidelberg: Springer Berlin

Heidelberg; 2014. p. 733–49. Available from: https://doi.org/10.1007/978-3-642-38954-2_126

38. Nelson W, Stegen J. The reduced genomes of Parcubacteria (OD1) contain signatures of a symbiotic lifestyle [Internet]. Vol. 6, Frontiers in Microbiology . 2015. p. 713. Available from: https://www.frontiersin.org/article/10.3389/fmicb.2015.00713

39. Yeoh YK, Sekiguchi Y, Parks DH, Hugenholtz P. Comparative Genomics of Candidate Phylum TM6 Suggests That Parasitism Is Widespread and Ancestral in This Lineage. Mol Biol Evol. 2016 Apr;33(4):915–27.

40. Pagani I, Lapidus A, Nolan M, Lucas S, Hammon N, Deshpande S, et al. Complete genome sequence of Desulfobulbus propionicus type strain (1pr3(T)). Stand Genomic Sci [Internet]. 2011 Mar 4;4(1):100–10. Available from: http://www.ncbi.nlm.nih.gov/pmc/articles/PMC3072085/

41. El Houari A, Ranchou-Peyruse M, Ranchou-Peyruse A, Dakdaki A, Guignard M, Idouhammou L, et al. Desulfobulbus oligotrophicus sp. nov., a sulfate-reducing and propionate-oxidizing bacterium isolated from a municipal anaerobic sewage sludge digester. Int J Syst Evol Microbiol [Internet]. 2017;67(2):275–81. Available from: http://ijs.microbiologyresearch.org/content/journal/ijsem/10.1099/ijsem.0.001615

42. Meyer B, Kuehl J V, Deutschbauer AM, Arkin AP, Stahl DA. Flexibility of Syntrophic Enzyme Systems in Desulfovibrio Species Ensures Their Adaptation Capability to Environmental Changes. J Bacteriol [Internet]. 2013 Nov 1;195(21):4900–14. Available from: http://jb.asm.org/content/195/21/4900.abstract

43. Copeland A, Spring S, Göker M, Schneider S, Lapidus A, Del Rio TG, et al. Complete genome sequence of Desulfomicrobium baculatum type strain (X(T)). Stand Genomic Sci [Internet]. 2009 Jul 20;1(1):29–37. Available from: http://www.ncbi.nlm.nih.gov/pmc/articles/PMC3035215/

44. Ofiţeru ID, Lunn M, Curtis TP, Wells GF, Criddle CS, Francis CA, et al. Combined niche and neutral effects in a microbial wastewater treatment community. Proc Natl Acad Sci [Internet]. 2010 Aug 31;107(35):15345 LP-15350. Available from: http://www.pnas.org/content/107/35/15345.abstract

Author Contributions

ACT, SC, UZI and GC, designed the study. ACT performed all of the physico-chemical characterisation with assistance from CM and SM. IB and GG collaborated on EPS measurements and characterisation. ACT prepared the sequencing libraries. UZI wrote the scripts for data analysis, which was conducted by ACT. CQ contributed to application of ecological theory. Results were interpreted by ACT, IB, GG, UZI and GC. ACT drafted the paper and CQ, UZI and GC revised the document. UZI and GC are joint corresponding authors. All authors approve the paper and agree for accountability of the work therein.

Competing Interests Statement

The authors declare no competing interests.

Acknowledgements

The authors thank NVP Energy for providing anaerobic sludge granules. SC was supported by the Engineering and Physical Sciences Research Council, UK (EP/J00538X/1). CM was supported by Erasmus and by the University of Turin and NUI Galway. CQ was funded by an MRC fellowship MR/M50161X/1 as part of the CLoud Infrastructure for Microbial Genomics (CLIMB) consortium MR/L015080/1. UZI was funded by NERC IRF NE/L011956/1. GC, SM and ACT were supported by a European Research Council Starting Grant (3C-BIOTECH 261330) and by a Science Foundation Ireland Career Development Award to GC. ACT was further supported by a Thomas Crawford Hayes bursary from NUI Galway, and to visit IB and GG by a Short-Term Scientific Mission grant through the EU COST Action 1302.

LEGENDS TO THE FIGURES

Figure 1. Physico-chemical and physiological data from granule size fractions, A – J. **(a)** Bar plot indicating the size ranges of respective fractions, along with relative volumetric contributions to the sludge; **(b)** VS proportions of TS; **(c)** typical scanning electron microscopy (SEM) micrographs of selected granules (from fractions B, D, F, H and J); **(d)** scatter plot illustrating density, and settling velocity, of granules (*n*=10) from each size fraction; **(e)** heat map depicting specific methanogenic activity (SMA) of sludge samples (*n*=3) from each size fraction (except fraction J) against acetate (Ace), propionate (Prop), butyrate (Buty) and H_2/CO_2 (Hyd); and **(f)** stacked bar charts showing relative concentrations of proteins, humic-like substances (HLS) and polysaccharides

710 components in loosely-bound and tightly-bound-EPS extracted from each size fraction
711 (except fraction J).
712
713 **Figure 2.** Microbial diversity, and community structure, in samples (*n*=3) from across
714 each of the ten size fractions, A-J*,* according to variances in the 16S rRNA gene. *Alpha*
715 *diversity*: box plot of the **(a)** rarefied species richness and **(b)** Shannon Entropy. *Beta*
716 *diversity*: Non-Metric Multidimensional Scaling (NMDS) using **(c)** Bray-Curtis
717 dissimilarity and **(d)** weighted UniFrac distances, where each point corresponds to the
718 community structure of one sample, size fractions are indicated by colour, and the
719 ellipses are drawn at a 95% CI; **(e)** community structure based on relative abundance of
720 the top-25 most abundant OTUs from across each size fraction, where 'others' refers to
721 all OTUs not included in the 'top-25'; *Environmental Filtering:* **(f)** Net Relatedness Index
722 (NRI) and **(g)** Nearest Taxa Index (NTI) calculated using the phylogenetic tree with
723 presence/absence abundance; **(h)** depiction of the proposed granule growth trajectory,
724 where the dashed line shows the proposed, closed life cycle. Lines for figures a, b, f & g
725 connect two categories where the differences were significant (ANOVA) with * ($P < 0.05$),
726 ** ($P < 0.01$), or *** ($p < 0.001$).
727
728 **Figure 3.** Heatmap of the discriminant OTUs across the ten size fractions (A – J; in
729 triplicate, *n*=30) identified using sPLS-DA analysis with both rows and columns ordered
730 using hierarchical (average linkage) clustering to identify blocks of OTUs of interest.
731 Heatmap depicts TSS+CLR normalised abundances: high abundance (red) and low
732 abundance (blue).

733

734 **Figure 4. (a)** Correlation plot depicting the 155 significantly discriminant OTUs coloured
735 according to taxonomy (except where black), from sPLS analysis across the ten size
736 fractions binned into three size groups: small (fractions A-C), medium (fractions D-G)
737 and large (fractions H-J), and showing correlations with physico-chemical variables
738 calculated using the Kendall rank correlation coefficient, where significant positive (pink)
739 or negative (blue) correlations are marked with * (*Adj. P* < 0.05), ** (*Adj. P* < 0.01) or ***
740 (*Adj. P* < 0.001); and **(b)** bar charts of the number of discriminant OTUs (x-axis) from
741 major phyla that were found in small, medium, and large bins.

742

743 **Figure 5.** Plots showing that **(a)** as granules increase in size the fraction of
744 *Euryarcheota* (which are 85% of methanogens) increases; and **(b)** rarefied
745 *Euryarcheota* richness remains fixed with granule size.

746

747 **Figure S1.** SEM micrographs of representative granules from size fractions A – J.

748

749 **Figure S2.** Non-Metric Multidimensional Scaling (NMDS) using UniFrac distances,
750 where each point corresponds to the community structure of one sample, size fractions
751 are indicated by colour , and the ellipses are drawn at a 95% CI.

Figure 1.

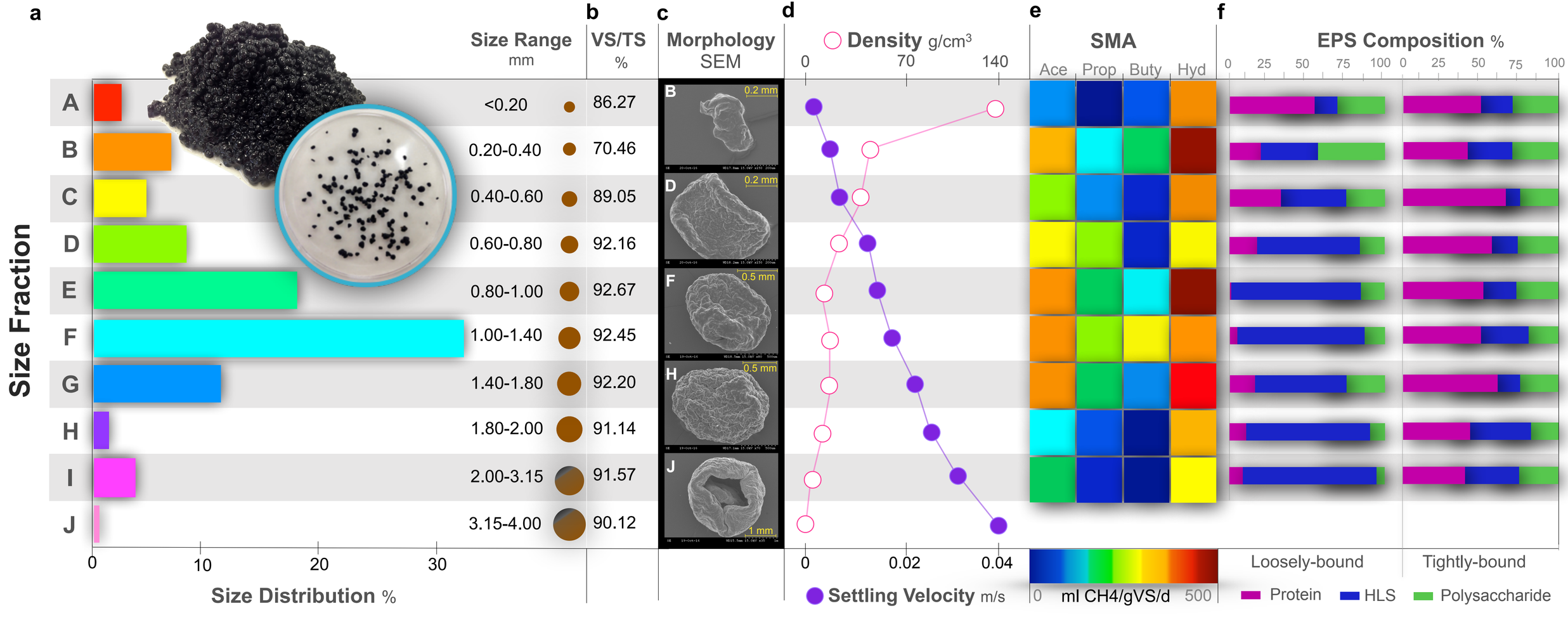
a
b
c
d
e
f
Size Range
mm
VS/TS
%
Morphology
SEM
Density g/cm3
SMA
Ace
Prop
Buty
Hyd
EPS Composition %
Size Fraction
A
B
C
D
E
F
G
H
I
J
<0.20
0.20-0.40
0.40-0.60
0.60-0.80
0.80-1.00
1.00-1.40
1.40-1.80
1.80-2.00
2.00-3.15
3.15-4.00
86.27
70.46
89.05
92.16
92.67
92.45
92.20
91.14
91.57
90.12
0.2 mm
0.5 mm
1 mm
0
10
20
30
Size Distribution %
0
70
140
0
0.02
0.04
Settling Velocity m/s
0
25
50
75
100
Loosely-bound
Tightly-bound
Protein
HLS
Polysaccharide
0
ml CH4/gVS/d
500

Figure 2.

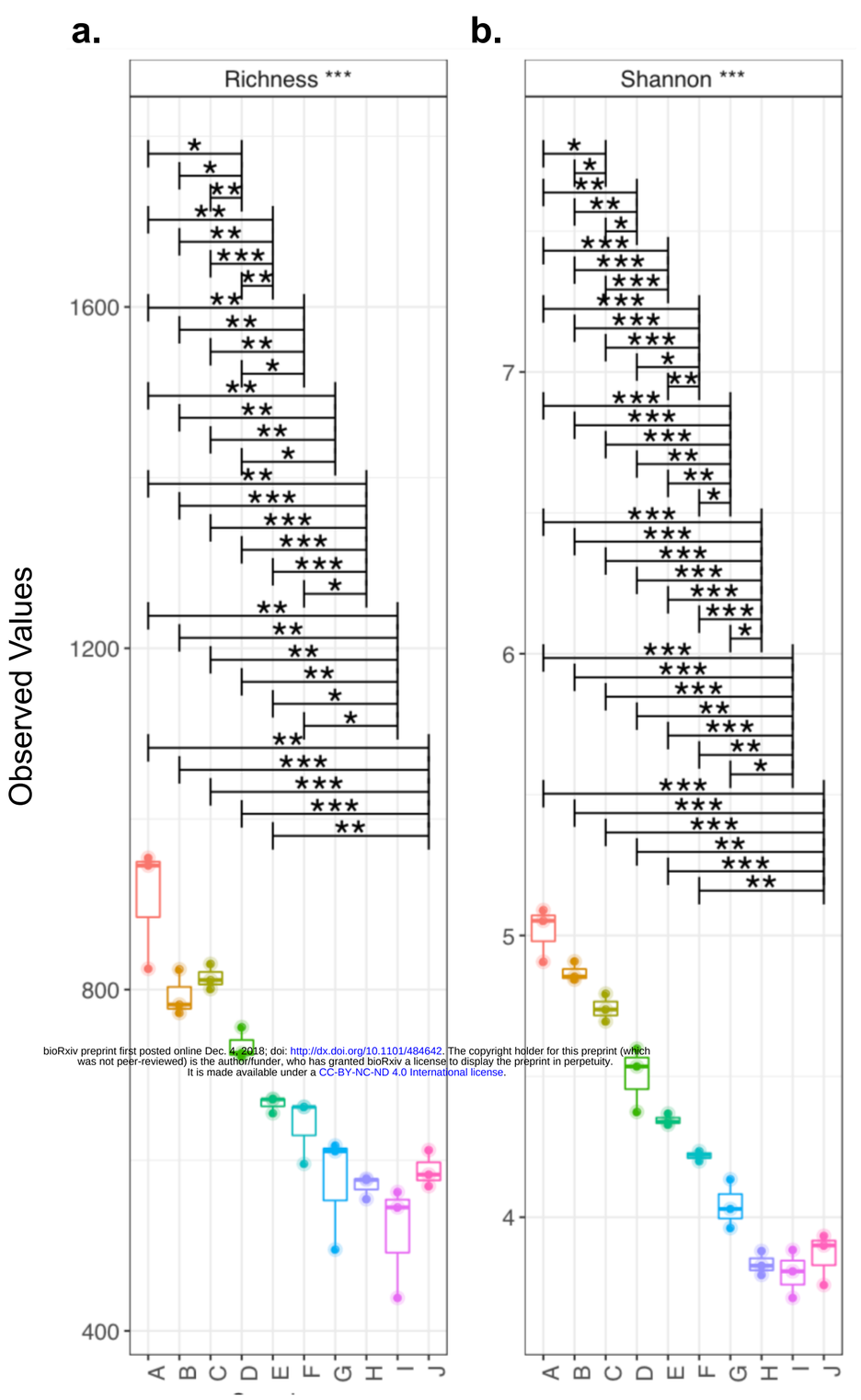

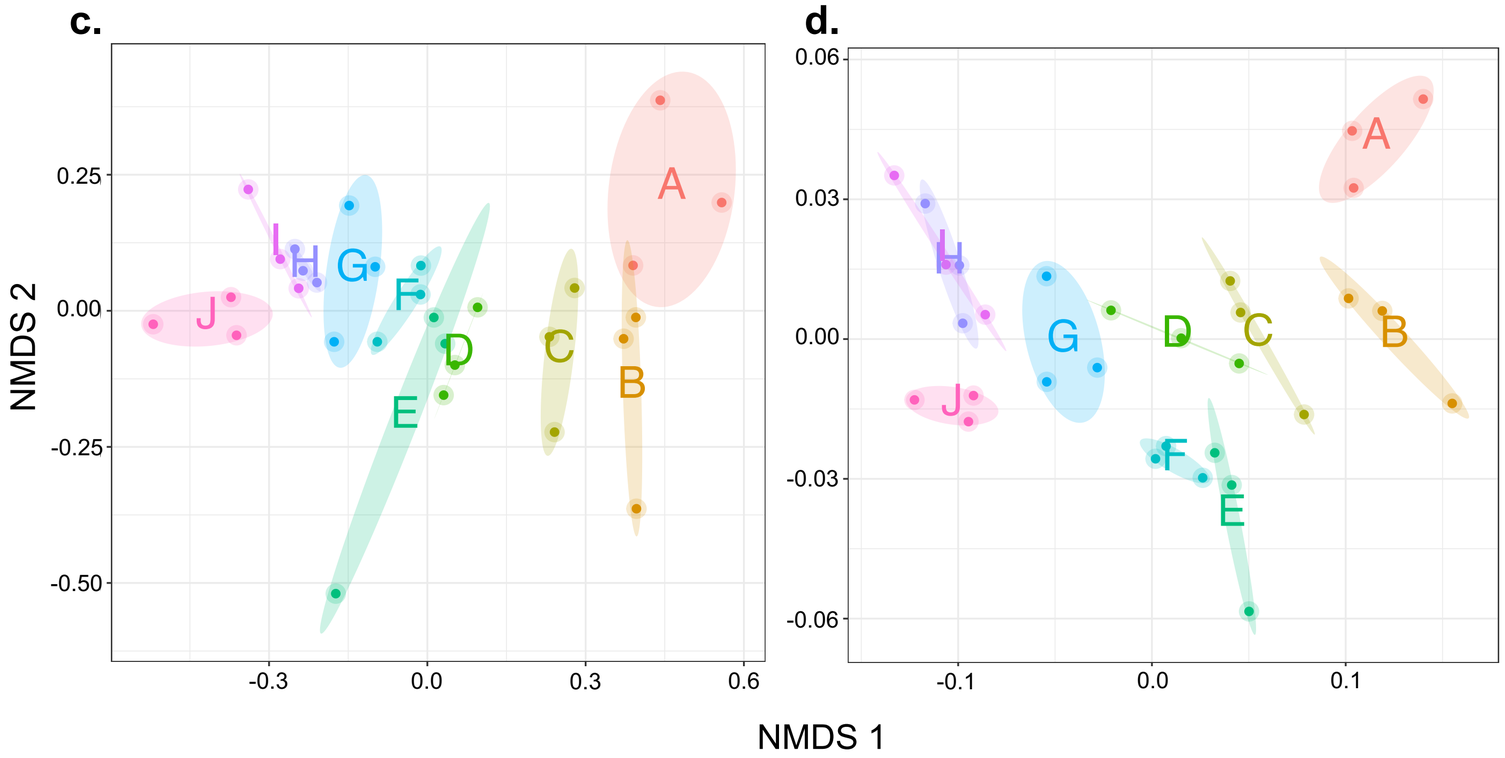

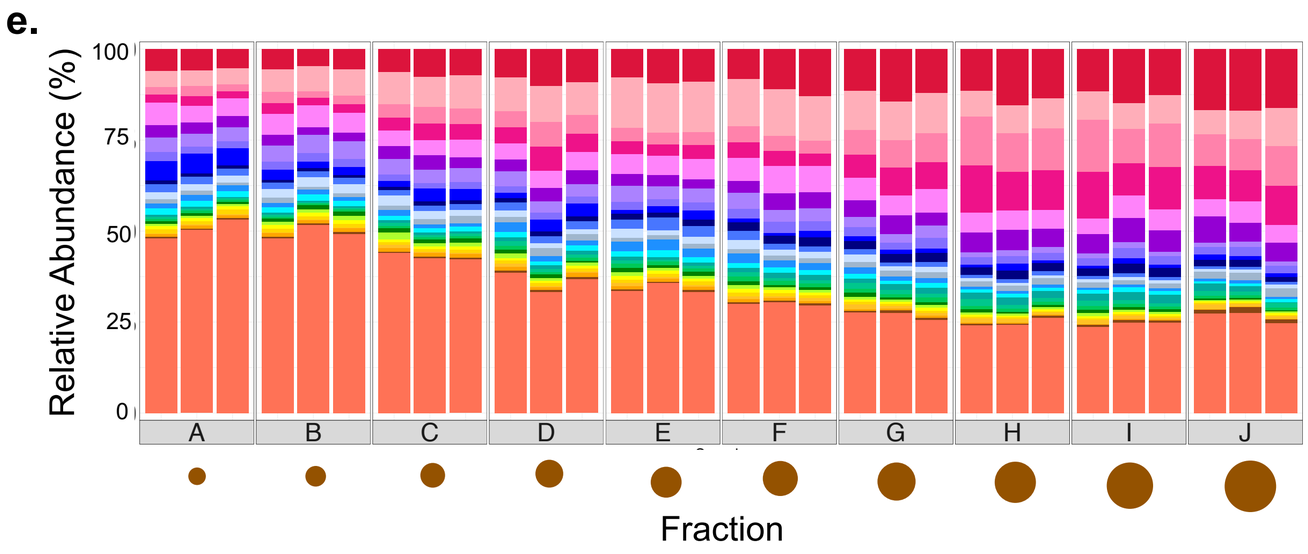

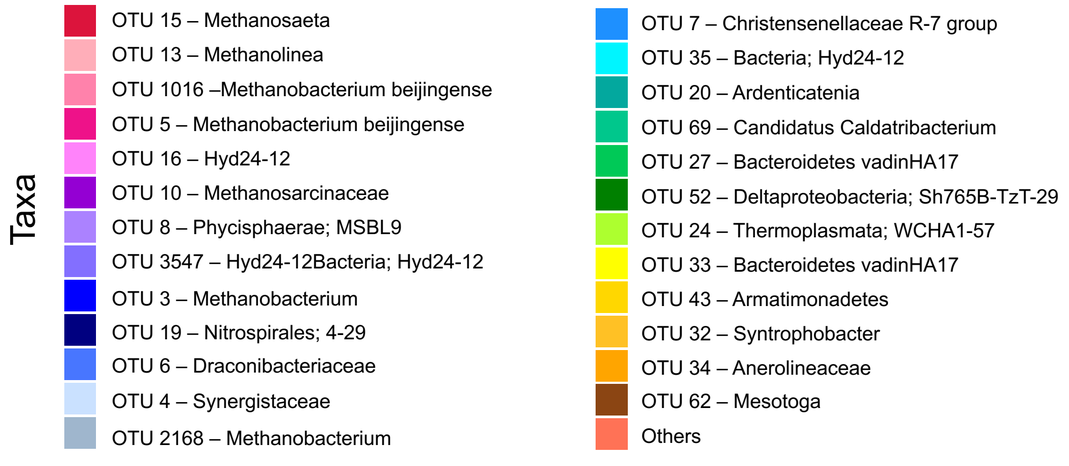

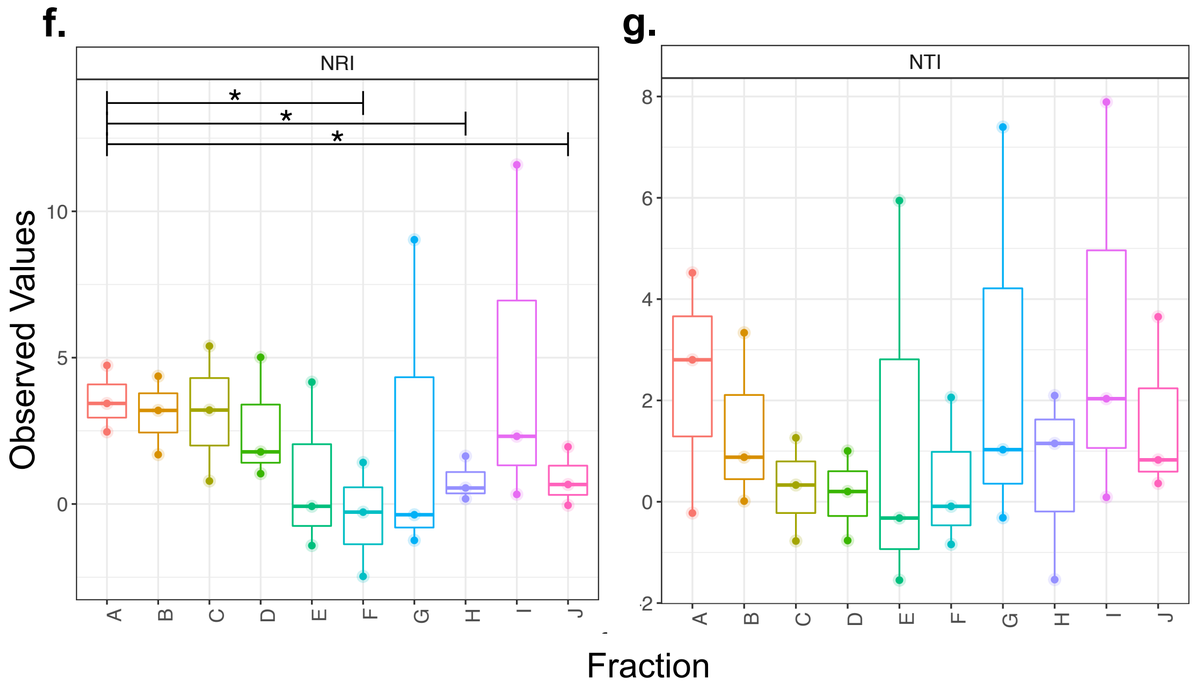

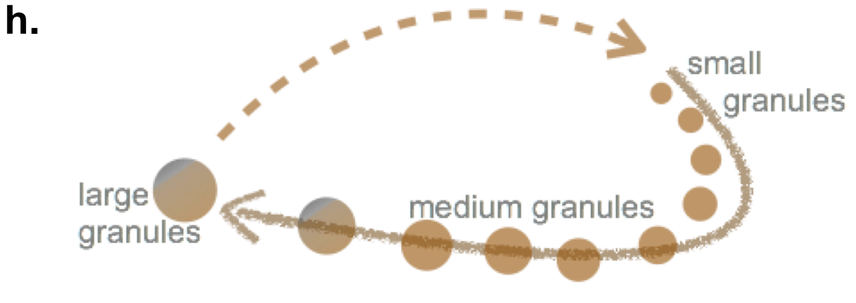

Figure 3.

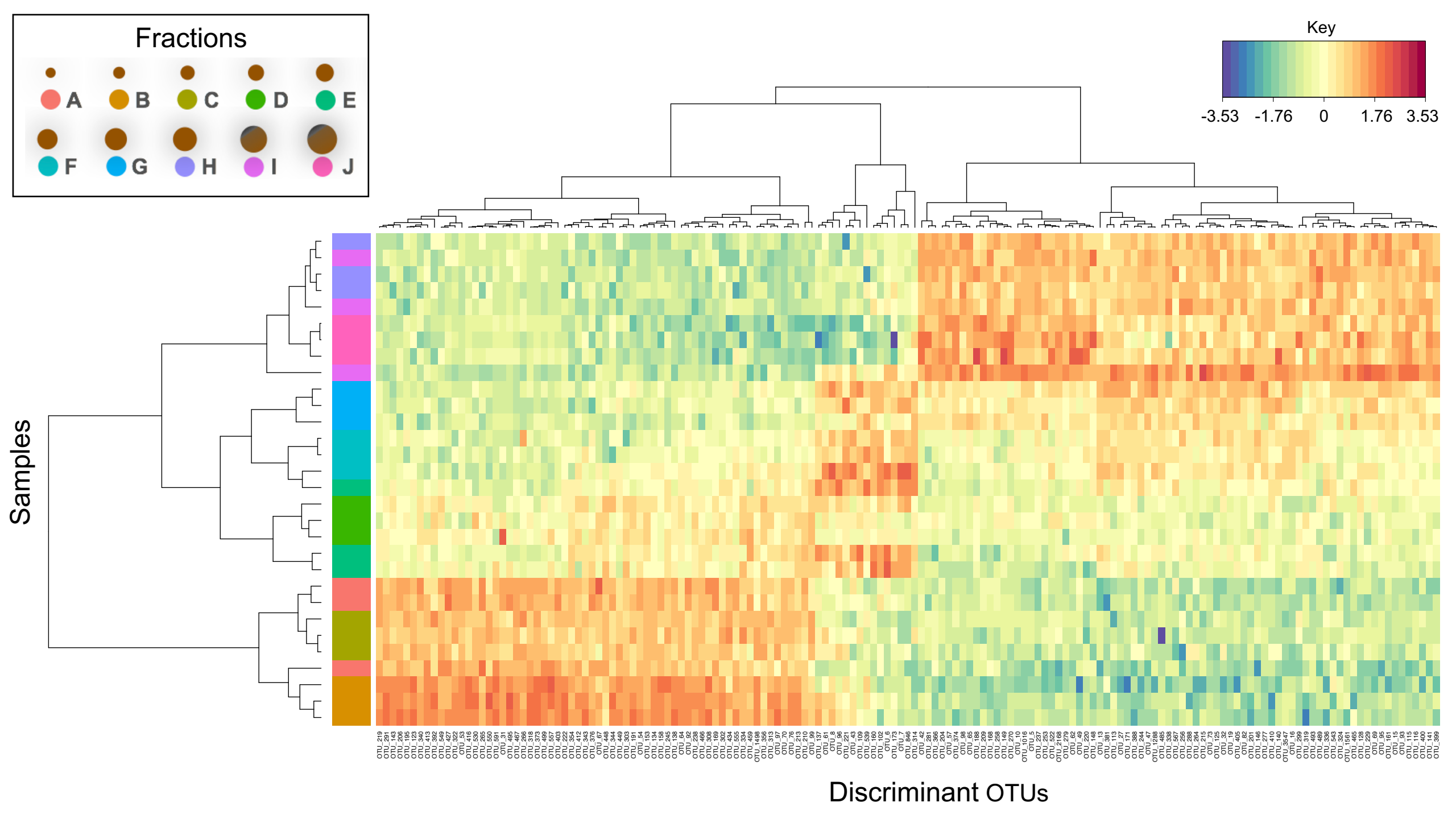
Fractions
A
B
C
D
E
F
G
H
I
J
Key
-3.53
-1.76
0
1.76
3.53
Samples
Discriminant OTUs

Figure 4.

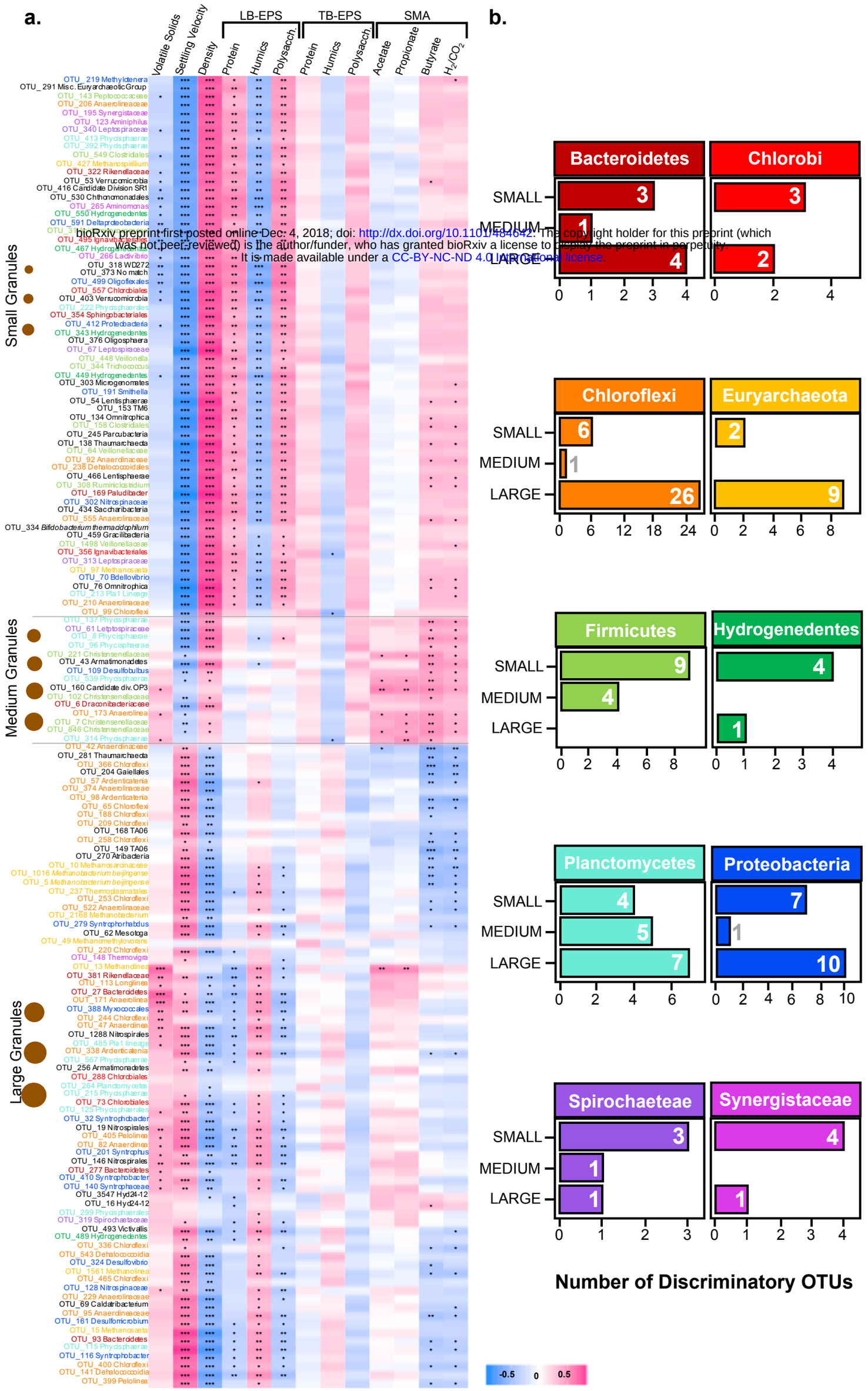

Figure 5.

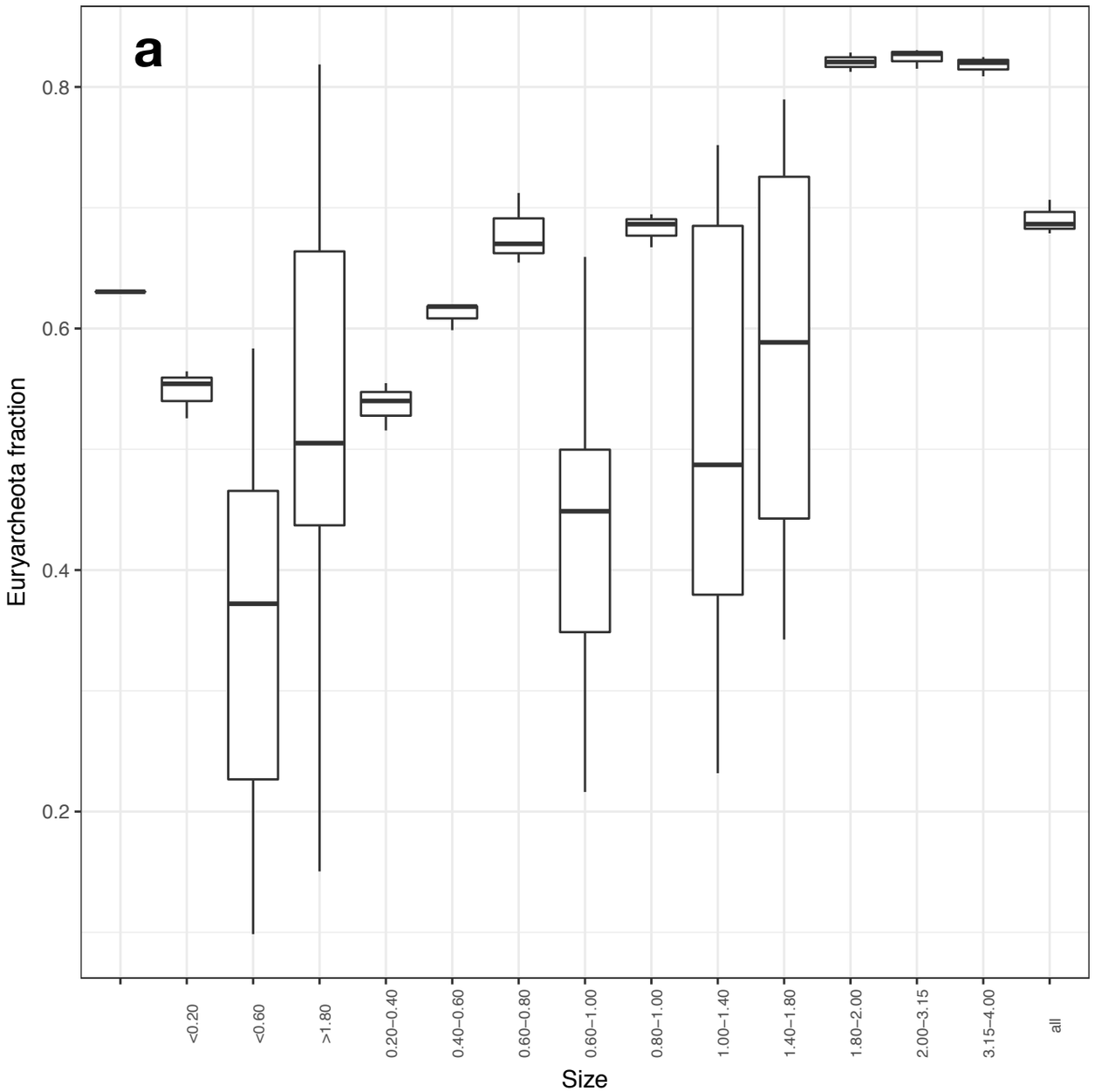

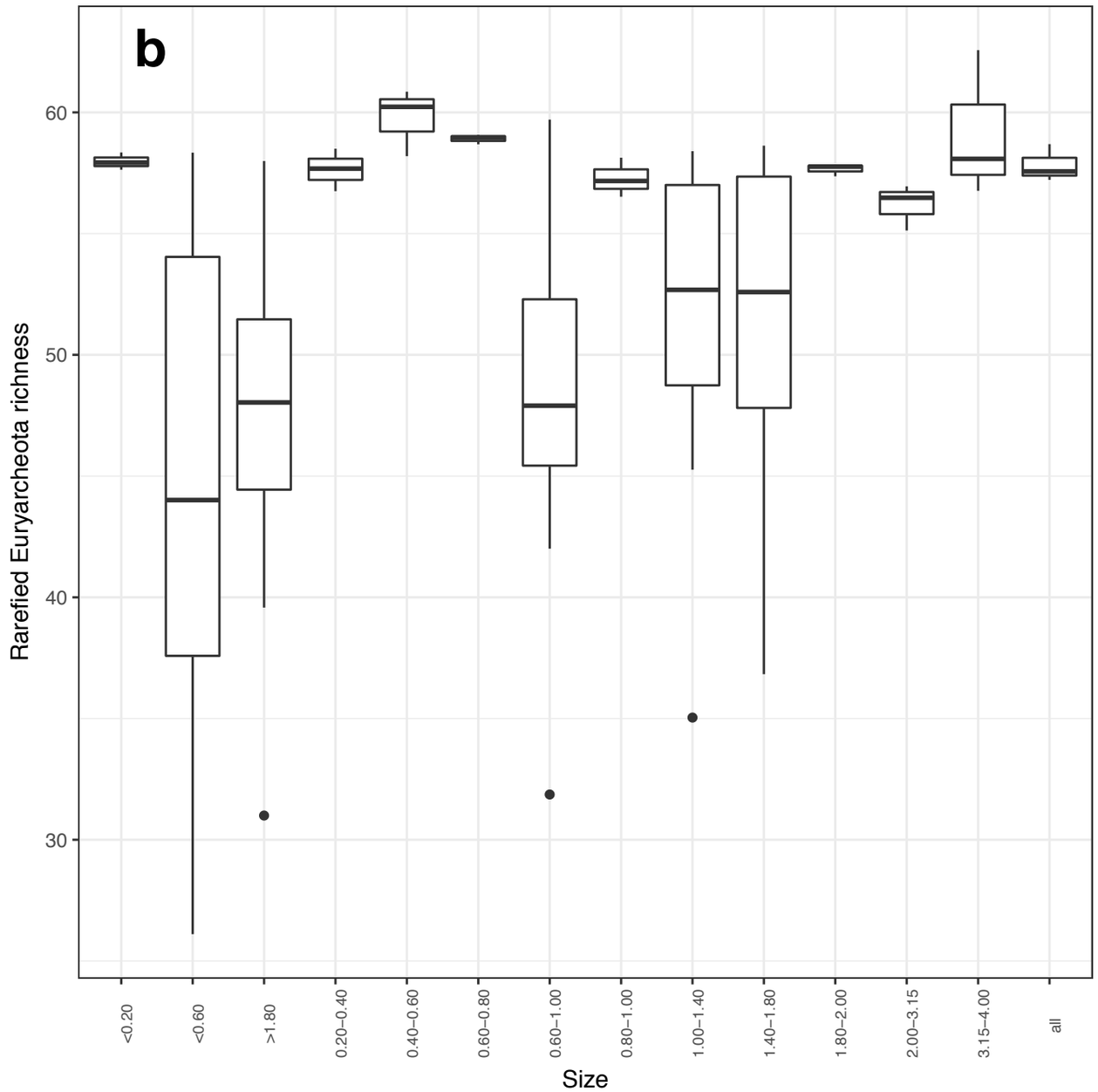

Figure S1.

Supplementary Figure 1.

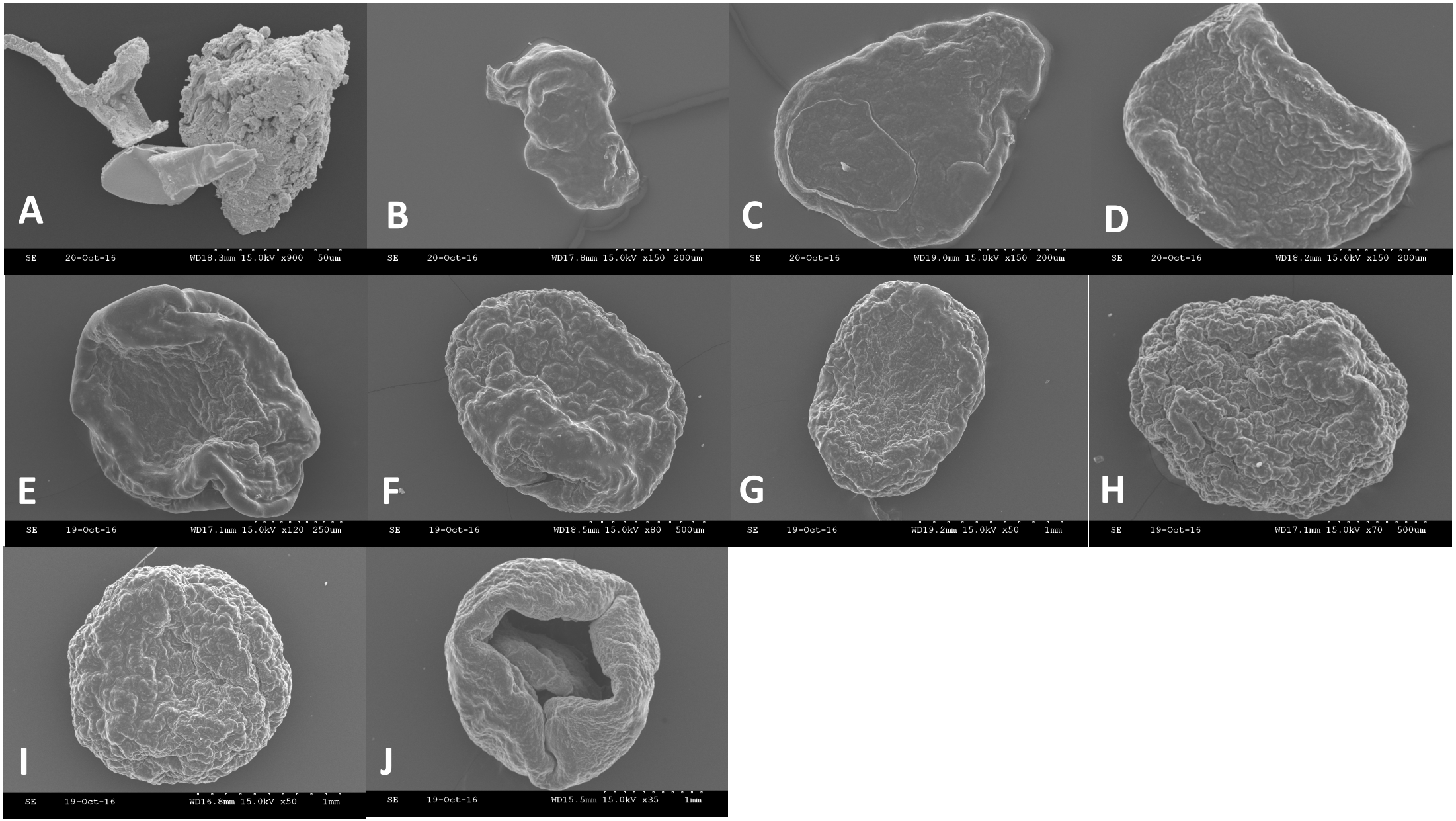
A
SE 20-Oct-16 WD18.3mm 15.0kV x900 50um
B
SE 20-Oct-16 WD17.8mm 15.0kV x150 200um
C
SE 20-Oct-16 WD19.0mm 15.0kV x150 200um
D
SE 20-Oct-16 WD18.2mm 15.0kV x150 200um
E
SE 19-Oct-16 WD17.1mm 15.0kV x120 250um
F
SE 19-Oct-16 WD18.5mm 15.0kV x80 500um
G
SE 19-Oct-16 WD19.2mm 15.0kV x50 1mm
H
SE 19-Oct-16 WD17.1mm 15.0kV x70 500um
I
SE 19-Oct-16 WD16.8mm 15.0kV x50 1mm
J
SE 19-Oct-16 WD15.5mm 15.0kV x35 1mm

Figure S2.

Supplementary Figure 2.

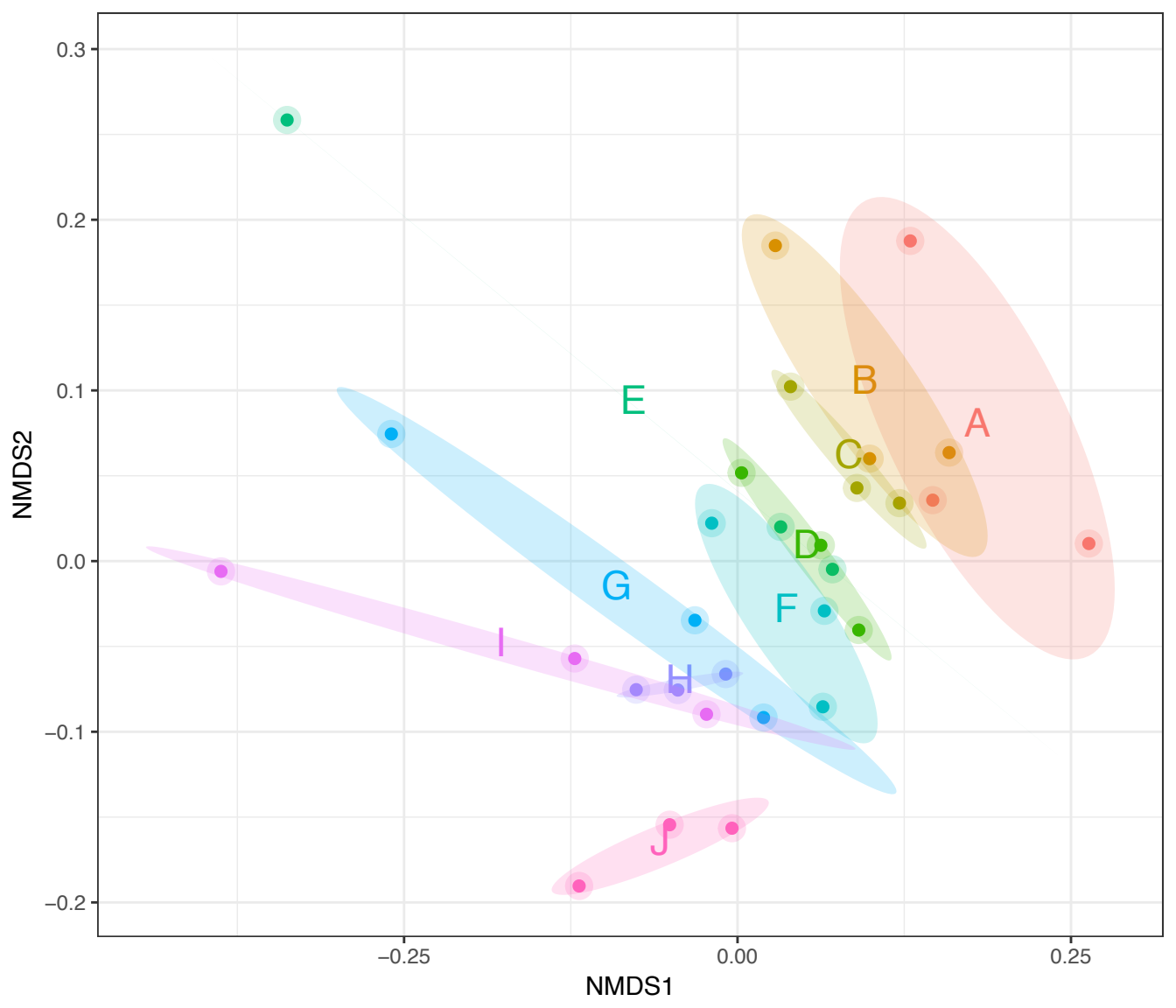
0.3
0.2
0.1
0.0
−0.1
−0.2
NMDS2
−0.25
0.00
0.25
NMDS1
A
B
C
D
E
F
G
H
I
J

DIVERSITY CONVERGES DURING COMMUNITY ASSEMBLY IN METHANOGENIC GRANULES, SUGGESTING A BIOFILM LIFE-CYCLE

Anna Christine Trego, Cristina Morabito, Simon Mills, Stephanie Connelly, Isabelle Bourven, Giles Guibaud, Christopher Quince, Umer Zeeshan Ijaz*, Gavin Collins*

**Joint correspondents:*

Umer Ijaz (umer.ijaz@glasgow.ac.uk) and Gavin Collins (gavin.collins@nuigalway.ie)

Supplementary Materials and Methods

Bioinformatics

Sickle v1.200 (1) was used to trim and filter paired-end reads. This software used a sliding window technique and trimmed regions where the average base quality dropped below 20. Next, a length threshold of 10 bp was used to discard reads that fell below this length. BayesHammer (2) was applied from the Spades v2.5.0 assembler, which error-corrected the paired-end reads. Following this, pandaseq v(2.4) was used to assemble the forward and reverse reads into a single sequence spanning the entire V3-V4 region with a minimum overlap of 20 bp. This provided consensus sequences for each sample. Recent work (3,4) has shown that this pipeline significantly reduces substitution rates (which is the primary type of error encountered in datasets generated by the Illumina MiSeq platform).

Next, VSEARCH (v2.3.4) was used for OTU construction (the steps are documented at http://github.com/torognes/vsearch/wiki/VSEARCH-pipeline). First, all reads from each sample were pooled together while barcodes were added to keep track of from which sample the read originated. The reads were then de-replicated, sorted in order of decreasing abundance, and singletons were discarded. Next, the reads were clustered based on 97% similarity, followed by removing clusters with chimeric models built from more abundant reads (--uchime_denovo option in vsearch). To remove any chimeras that may have been missed, particularly in the case that they had parents that were absent from the reads or were present in very low abundance, a reference-based chimera filtering step (--uchime_ref option in vsearch) using a gold database (https://www.mothur.org/w/images/f/f1/Silva.gold.bacteria.zip) was applied. Finally, the OTU table was generated by matching the original barcoded reads against clean OTUs (a total of 2927 OTUs for n=30 samples) at 97% similarity (a proxy for species-level separation).

The assign_taxonomy.py script from the Qiime workflow (5) was used to taxonomically classify the representative OTUs against the SILVA SSU Ref NR database release v123 database. Phylogenetic distances between OTUs were resolved using kalign v2.0.4 (6) as a multisequence alignment (options –gpo 11 –gpe 0.85). Following this, FastTree v2.1.7 (7) generated the phylogenetic tree in NEWICK format and biome files for the OTUs were generated by combining the abundance table with taxonomy information using make_otu_table.py from the Qiime workflow.

Statistical analyses

The vegan package (8) was used for alpha and beta diversity analyses. For alpha diversity measures we used: **(i)** *rarefied richness* – the estimated number of species/features in a rarefied sample (to minimum library size); **(ii)** *Shannon entropy* – a commonly used index to measure balance within a community; **(iii)** *Simpson index* – a measure of dominance that weighs towards the abundance of the most common OTUs and is less sensitive to rare(r) OTUs; **(iv)** *Pilou eveness,* which compares the actual diversity values to the maximum possible diversity value, and is constrained between 0 and 1.0, whereby lower values will indicate more variation in abundance between different OTUs in the community; and **(v)** *Fisher's alpha* – a parametric index of diversity that assumes the abundance of OTUs following the log series distribution. Non-metric multidimensional scaling (NMDS) plots of OTUs using three different distance measures were made using Vegan's metamds() function: **(1)** *Bray-Curtis,* which is a distance metric that considers only OTU abundance counts; **(2)** *Unweighted Unifrac,* which is a phylogenetic distance metric that calculates the distance between samples by taking the proportion of the sum of unshared branch lengths in the sum of all the branch lengths of the phylogenetic tree for the OTUs observed in two samples, and without taking into account their abundances; and **(3)** *Weighted Unifrac,* which is a phylogenetic distance metric combining phylogenetic distance with relative abundances. This places emphasis on dominant OTUs or taxa. Unifrac distances were calculated using the phyloseq package (9).

To understand multivariate homogeneity of group dispersions (variances) between multiple conditions, Vegan's betadisper() function was used, in which the distances between objects and group centroids were handled by reducing the original distances (BrayCurtis, Unweighted Unifrac, or Weighted Unifrac) to principal coordinates and then performing ANOVA on them. Analysis of variance was performed using Vegan's Adonis() against distance matrices (Bray-Curtis/Unweighted Unifrac/Weighted Unifrac). This function, refered to as PERMANOVA, fits linear models to distance matrices and used a permutation test with pseudo-F ratios.

Phylogenetic distances within each sample were further characterised by calculating the nearest taxa index (NTI) and net relatedness index (NRI). This analysis helped determine whether the community structure was stochastic (i.e. driven by competition among taxa) or deterministic (i.e. driven by strong environmental pressure). The NTI was calculated using mntd() and ses.mntd(), and the mean phylogenetic diversity (MPD) and NRI were calculated using mpd() and ses.mpd() functions from the picante package (10). NTI and NRI represent the negatives of the output from ses.mntd() and ses.mpd(), respectively. Additionally, they quantify the number of standard deviations that separate the observed values from the mean of the null distribution (999 randomisation using null.model-'richness' in the ses.mntd() and ses.mpd() functions and only considering taxa as either present or absent regardless of their relative abundance). The positive value of NTI indicates that species co-occur with more closely related species than expected by chance, with negative values suggesting otherwise. NTI measures tip-level divergences (putting more emphasis on terminal clades and is akin to "local" clustering) in phylogeny

while NRI measures deeper divergences (akin to “global” clustering or “clumpedness”). For both NTI and NRI, values > +2 indicate strong environmental pressure, and values < -2 indicate strong competition among species as the driver of community structure. Based upon the recommendations given by Stegen *et al*. (11) we used only the top 1,000 most abundant OTUs for the calculations.

Sparse Projection to Latent Structure – Discriminant Analysis (sPLS-DA) was performed using the MixOmics package for R (12). This analysis constructed artificial latent components for predicted variables OTUs and response variables (categorical data matrix of different size fractions) by factoring these matrices into *scores* and *loading vectors* in a new space to achieve a maximum covariance between the scores of these two matrices. The loading vectors (with piece-wise coefficient for each OTU) were constructed so that the coefficients indicate the importance of each variable to define the component. Any non-zero coefficients for the loading vectors indicate genera that very significantly between the categories and are deemed discriminants. The OTU table was initially prefiltered by removing 1% of OTUs with low counts as based on author’s recommendation given at http://mixomics.org/mixmc/pre-processing/. After this step, we normalised the OTU table using Total Sum Scaling (TSS) on the OTUs followed by Centered Log Ratio (CLR), collectively referred to as TSS+CLR normalisation, and before applying the *splsda*() function. The *perf*.*plsda*() and *tune*.*splsda*() functions were initially used to predict the number of latent components (associated loading vectors) and the number of discriminants by initializing the *perf*.*plsda*() procedure with the total number components to be the number of size fractions considered in this study and then retaining

the first two components as the classification error rates were minimum for these (<10%) using the centroid distance matrix in the procedure. The tune.splsda() function was then initialized with two components and using 5-fold cross-validation with 10 repeats (i.e. splitting the data into training and testing sets) identified the 155 discriminant OTUs amongst the size fraction. In both procedures we considered two metrics for classification error rates: the overall error rates and the balanced error rates (BER). Balanced error rates are measured between the predicted latent variables and the centroid of the class labels (size fractions considered in the study). BER accounts for differences in the number of samples between different size fractions. The OTUs that were deemed to be discriminants in the sPLS-DA analysis were selected and further analysed by determining correlations with external parameters (environmental meta data) using Kendall rank correlation with P-values adjusted for multiple comparisons using the Benjamini-Hochberg correction (13).

References

1. Joshi N, Fass J. Sickle: A sliding-window, adaptive, quality-based trimming tool for FastQ files (Version 1.33). 2011.
2. Nikolenko SI, Korobeynikov AI, Alekseyev MA. BayesHammer: Bayesian clustering for error correction in single-cell sequencing. BMC Genomics [Internet]. 2013 Jan;14(1):S7. Available from: https://doi.org/10.1186/1471-2164-14-S1-S7
3. Schirmer M, Ijaz UZ, D'Amore R, Hall N, Sloan WT, Quince C. Insight into biases and sequencing errors for amplicon sequencing with the Illumina MiSeq platform. Nucleic Acids Res. 2015;43(6).

4. D'Amore R, Ijaz UZ, Schirmer M, Kenny JG, Gregory R, Darby AC, et al. A comprehensive benchmarking study of protocols and sequencing platforms for 16S rRNA community profiling. BMC Genomics [Internet]. 2016 Jan;17(1):55. Available from: https://doi.org/10.1186/s12864-015-2194-9

5. Caporaso JG, Kuczynski J, Stombaugh J, Bittinger K, Bushman FD, Costello EK, et al. QIIME allows analysis of high-throughput community sequencing data. Nat Methods [Internet]. 2010 Apr 11;7:335. Available from: http://dx.doi.org/10.1038/nmeth.f.303

6. Lassmann T, Sonnhammer ELL. Kalign -- an accurate and fast multiple sequence alignment algorithm. BMC Bioinformatics [Internet]. 2005 Dec;6(1):298. Available from: https://doi.org/10.1186/1471-2105-6-298

7. Price MN, Dehal PS, Arkin AP. FastTree 2 – Approximately Maximum-Likelihood Trees for Large Alignments. PLoS One [Internet]. 2010 Mar 10;5(3):e9490. Available from: https://doi.org/10.1371/journal.pone.0009490

8. Oksanen J, Blanchet F, Kindt R, Legendre P, Minchin PR, O'hara R, et al. Vegan: community ecology package. R Package version 2.2-1. 2015.

9. McMurdie PJ, Holmes S. phyloseq: An R Package for Reproducible Interactive Analysis and Graphics of Microbiome Census Data. PLoS One [Internet]. 2013 Apr 22;8(4):e61217. Available from: https://doi.org/10.1371/journal.pone.0061217

10. Kembel SW, Cowan PD, Helmus MR, Cornwell WK, Morlon H, Ackerly DD, et al. Picante: R tools for integrating phylogenies and ecology. Bioinformatics [Internet]. 2010 Jun 1;26(11):1463–4. Available from: http://dx.doi.org/10.1093/bioinformatics/btq166

11. Stegen JC, Lin X, Konopka AE, Fredrickson JK. Stochastic and deterministic assembly processes in subsurface microbial communities. Isme J [Internet]. 2012 Mar 29;6:1653. Available from: http://dx.doi.org/10.1038/ismej.2012.22

12. Rohart F, Gautier B, Singh A, Lê Cao K-A. mixOmics: An R package for 'omics feature selection and multiple data integration. PLOS Comput Biol [Internet]. 2017 Nov 3;13(11):e1005752. Available from: https://doi.org/10.1371/journal.pcbi.1005752

13. Benjamini Y, Hochberg Y. Controlling the False Discovery Rate: A Practical and Powerful Approach to Multiple Testing. J R Stat Soc Ser B [Internet]. 1995;57(1):289–300. Available from: http://www.jstor.org/stable/2346101